Biosensors and Bioelectronics 25 (2009) 668–673

Contents lists available at ScienceDirect

Biosensors and Bioelectronics

journal homepage: www.elsevier.com/locate/bios

Electrochemical sensing the DNA damage *in situ* induced by a cathodic process based on $Fe@Fe_2O_3$ core–shell nanonecklace and Au nanoparticles mimicking metal toxicity pathways *in vivo*

Xueliang Wang, Tao Yang, Kui Jiao *

Key Laboratory of Eco-chemical Engineering (Ministry of Education), College of Chemistry and Molecular Engineering, Qingdao University of Science and Technology, Qingdao 266042, China

ARTICLE INFO

Article history:
Received 25 January 2009
Received in revised form 16 April 2009
Accepted 17 April 2009
Available online 24 April 2009

Keywords:
DNA damage
Electro-Fenton reaction
$Fe@Fe_2O_3$ core–shell nanonecklace
Au nanoparticle
Electrochemical sensing
In situ

ABSTRACT

Sensitive electrochemical sensing for the DNA damage *in situ* based on a cathodic process of $Fe@Fe_2O_3$ core–shell nanonecklace and Au nanoparticles was performed by a novel biosensor, which was constructed via a glassy carbon electrode (GCE) modified with a multilayer film comprising of separate layers of poly(dimethyldiallylammonium chloride) (PDDA), the mixture of $Fe@Fe_2O_3$ core–shell nanonecklace and Au nanoparticles, PDDA and double strand DNA (ds-DNA). Iron ions and H_2O_2 (Fenton reagents) were generated continuously at a constant rate by the cathodic process. The two Fenton reagents reacted further to generate hydroxyl radicals *in situ*, which attacked ds-DNA in the film and caused severe damage of ds-DNA molecules. These courses of DNA damage were just like those happened in organism. It could be used to mimic metal toxicity pathways *in vivo*. $Fe@Fe_2O_3$ core–shell nanonecklace and Au nanoparticles played considerable synergistic effects for DNA damage. Differential pulse voltammetry and cyclic voltammetry were applied to monitor the DNA damage. Different from the previously reported metal-mediated DNA damage sensor, the process of the ds-DNA damage was not achieved in the solution of metal ions and H_2O_2, but merely in buffer solution, and the instable enzymes were not used in the whole course. The biosensor possesses the potential as a screening tool for rapid assessment of the genotoxicity of existing and new chemicals.

1. Introduction

It is known to all that the new chemicals are being annually synthesized at an increasing rate. However, the potential deleterious effect on human and ecosystem of many existing and new chemicals is still unknown. Many heavy metals and organic compounds have been found to possess carcinogenic toxicity. The heavy metals induce their toxic effects primarily through production of reactive oxygen species (ROS) (frequently via Fenton-type reactions) to cause DNA oxidation, and the organic compounds or their *in vivo* metabolites through the formation of DNA adducts (Shosuke et al., 2002; Xue and Warshawsky, 2005), respectively. Methods for detecting DNA damage could serve as effective screening for the toxicity of the chemicals at an early point in their commercial development and as an effective means for checking genetic disease. Therefore, there is an urgent demand for rapid detection of the DNA damage for effective screening for the toxicity of a large number of existing and new chemicals.

The DNA damage products have been identified and quantified by a number of analytical techniques (Tarun and Rusling, 2005; Tarun et al., 2006), such as gas chromatography/mass spectrometry, high-performance liquid chromatography (HPLC)/electrochemistry and a combination with mass spectrometry, ^{32}P-postlabeling, gel electrophoresis and immunoassays. Although these methods are powerful for detection of DNA damage, their limitations are also obvious. For example, gel electrophoresis is limited only to detect some classes of lesions due to its inherent characteristics. HPLC/electrochemistry and ^{32}P-postlabeling require hydrolysis of sample DNA, which can decrease the signal-to-noise ratio and alter the chemical structure. Recently, electrochemical, photoelectrochemical and chemiluminescent sensors and sensor arrays (Zhou et al., 2003; Mugweru et al., 2004; So et al., 2008; Palecék et al., 1998; Liang and Guo, 2007; Liang et al., 2008) have been applied for the DNA damage detection. In these methods, many bioactive proteins such as cytochrome P450, hemoglobin (Hb) and myoglobin (Mb) were incorporated into the sensor film to mimic the *in vivo* toxicity pathway. These proteins in the film were activated in H_2O_2 solution to convert styrene into the DNA-reactive form, styrene oxide. In order to avoid the use of the instable H_2O_2 directly for mimicking the metal-mediated DNA damage pathway *in vivo*, Liang et al.

* Corresponding author. Tel.: +86 532 84855977; fax: +86 532 84023927.
E-mail address: kjiao@qust.edu.cn (K. Jiao).

0956-5663/$ – see front matter.
doi:10.1016/j.bios.2009.04.026

(2008) embedded glucose oxidase into the multicomponent photoelectrochemical sensing film when the sample solution contained Fe^{2+} and glucose. H_2O_2 was generated *in situ* in the reaction process.

In this paper, in order to mimic the metal-mediated DNA damage *in vivo*, a novel electrochemical biosensor was developed by incorporating the mixture of Fe@Fe_2O_3 core–shell nanonecklace and Au nanoparticles into a multicomponent film containing double strand DNA (ds-DNA). When the biosensor was treated using a cathodic process, the iron ions could be generated by slowly leaking from the Fe@Fe_2O_3 nanonecklace and H_2O_2 by the reduction of O_2 on the Au nanoparticles *in situ* at a constant rate. The iron ions and H_2O_2 reacted further to generate hydroxyl radicals *in situ*, which could induce several classes of DNA damage, including single-strand break, double-strand break, abasic sites, and base oxidation both *in vitro* and *in vivo* (Jia et al., 2008; Cooke et al., 2003). Then the DNA damage was detected by using two electroactive indicators, $Ru(NH_3)_6^{3+}$ and $Co(phen)_3^{3+}$, with the differential pulse voltammetry (DPV). To best of our knowledge, this is the first sensor to mimic the metal-mediated DNA damage pathways by a process of cathodic treatment. This biosensor has the potential as a screening tool for the rapid assessment of the genotoxicity of existing and new chemicals.

2. Experimental

2.1. Apparatus

The electrochemical experiments were carried out using a CHI 660 C electrochemical workstation (Shanghai CH Instruments, China) with a three-electrode arrangement consisting of a glassy carbon electrode (GCE) or film-coated GCE working electrode, a saturated calomel reference electrode (SCE) and a platinum wire auxiliary electrode. Scanning electron microscopy (SEM) images and transmission electron microscopy (TEM) images were performed on a JEM-2000EM scanning electron microscope (JEOL, Japan) and a JSM-6700 transmission electron microscope (JEOL, Japan), respectively. X-ray powder diffraction (XRD) patterns of the samples were obtained on a D/MAX-rA X-ray diffractometer (Rigaku, Japan). The UV–vis absorption spectra were obtained on a Cary 50 probe spectrophotometer (Varian, Australia). The DNA damage by cathodic treatment processes was performed using a potentiostat/galvanostat (Shenzhen Zhaoxin Electronic Equipments & Instruments Producer, China). The pH values of all solutions were measured with a pHS-25C acidometer (Shanghai Leici Instrument Factory, China). 18.2 MΩ cm ultrapure water was prepared with an Aquapro AWL-1002-P (Ever Young Enterprises Development Co., Ltd., China).

2.2. Reagents

Herring sperm DNA (ds-DNA) and poly(dimethyldiallylammonium chloride) (PDDA) were purchased from Sigma, and $Ru(NH_3)_6Cl_3$ from Aldrich. Au nanoparticles and $Co(phen)_3(ClO_4)_3{\cdot}3H_2O$ were synthesized according to the published procedures (Storhoff et al., 1998; Dollimore and Gillard, 1973), respectively. The average size of Au nanoparticles is about 14 nm. Fe@Fe_2O_3 core–shell nanonecklace was synthesized by the reaction between ferric chloride and sodium borohydride according to the reference (Ai et al., 2007a). In detail: 0.15 g of $FeCl_3{\cdot}6H_2O$ was dissolved in 50 mL of ultrapure water to form a ferric solution (solution 1) and 0.3 g of $NaBH_4$ was added to 20 mL of ultrapure water to form solution 2. Solution 2 was then dropped into solution 1 at rate of 0.5 mL s^{-1}. During the addition, the fluffy black precipitates appeared on the surface of the solution. The fluffy black precipitates were washed with ultrapure water and ethanol, and finally dried under nitrogen ambience. All reagents are of analytical grade and used without further purification. Solutions were prepared with ultrapure water.

2.3. Procedure

2.3.1. Film construction

After the GCE had been pretreated according to the reference (Feng et al., 2008), the sensor film was constructed by sequentially covering GCE with PDDA, the mixture of Fe@Fe_2O_3 core–shell nanonecklace and Au nanoparticles with a volume ratio of 10:30, PDDA and ds-DNA. The concentrations of PDDA, Fe@Fe_2O_3 core–shell nanonecklace, Au nanoparticles and ds-DNA were 2.0 mg mL^{-1},

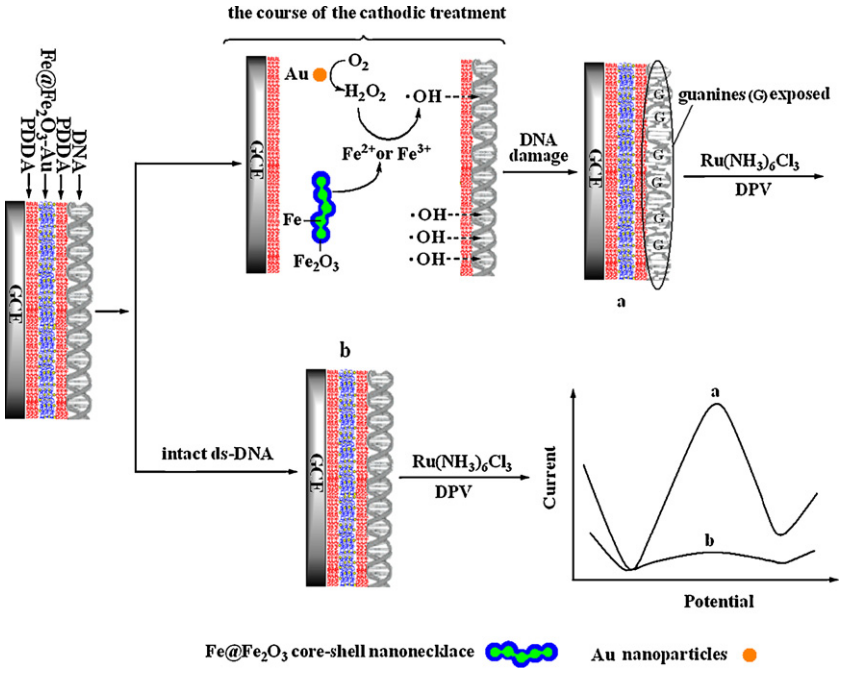

Scheme 1. Schematic diagram of the DNA damage detection method based on the cathodic treatment process.

1.5 mg mL^{-1}, 3.0×10^{-9} mol L^{-1} and 2.0 mg mL^{-1}, respectively, and the used amount of each layer was all 8.0 μL. The electrode was gently washed with water and air-dried naturally at room temperature after every casting. The ds-DNA could be easily immobilized on the film owing to the electrostatic force between the PDDA and ds-DNA. The modified electrode was denoted as DNA/PDDA/Fe@Fe_2O_3–Au/PDDA/GCE. Scheme 1 shows the build-up process of the sensor and the detection method of DNA damage induced by cathodic treatment process. During the course of the cathodic treatment, the iron ion was generated by slowly leaking from Fe@Fe_2O_3 core–shell nanonecklace, and H_2O_2 by oxygen reduction on the Au nanoparticle surface, respectively. Then the iron ion and H_2O_2 reacted further to produce •OH. The •OH attacked the DNA in the film and induced DNA damage *in situ*. The DPV peak current difference between after (Scheme 1a) and before (Scheme 1b) the DNA damage with $Ru(NH_3)_6^{3+}$ as the probe was used as the measurement signal for the DNA damage.

2.3.2. DNA damage and electrochemical measurements

The DNA damage was performed in 0.1 mol L^{-1} phosphate buffer solution (PBS) of pH 5.5 with the modified electrode as working cathode and Pt wire with a diameter of 0.05 mm as anode. The potential between the anode and cathode was controlled at 1.2 V. During the experiments, the cathode was fed with fresh air. After a given time, the electrode was taken out and rinsed with water.

The electrochemical measurements were conducted by recording differential pulse voltammogram of 50 mmol L^{-1} $Ru(NH_3)_6^{3+}$ or 20 mmol L^{-1} $Co(phen)_3^{3+}$ in 0.1 mol L^{-1} PBS of pH 5.5. DPV experiments were performed at a pulse amplitude of 10 mV, a pulse width of 100 ms and a pulse period of 300 ms. The scan potential range was from 1.2 V to 0.4 V for $Ru(NH_3)_6^{3+}$ and from 0.6 V to −0.4 V for $Co(phen)_3^{3+}$. The solution was purged with nitrogen and a nitrogen atmosphere was maintained during recording DPV curve.

3. Results and discussion

3.1. Characterization of Fe@Fe_2O_3 core–shell nanonecklace and film-coated electrode

The morphologies and microstructures of the as-prepared Fe@Fe_2O_3 nanonecklace were studied by field emission SEM and TEM. The results are shown in Fig. 1. It was found that the Fe@Fe_2O_3 nanonecklaces were loosely dispersed on the surface of the electrode and there were many pores, suggesting that the film could be easily penetrated by the electrolyte and gas components in solution, and provide plenty of sites for oxygen adsorption. The high-magnification SEM image revealed that the diameters of the nanonecklaces were 50–150 nm and the lengths several to several tens micrometers. From TEM images of the nanonecklace, it is obvious that the nanostructures were formed through connection of nanospheres one by one, looking like "pearl necklaces". So it was called "nanonecklace". Its gray edge and dark center were clearly observed, suggesting the core–shell structure of the nanosphere. The diameters of the core–shell nanonecklaces were about 50–150 nm, which was consistent with the SEM observation. The results of XRD (inset of Fig. 1A) exhibited that Fe and Fe_2O_3 were coexisted in the nanonecklace and the shell was Fe_2O_3, which was produced by the oxidation of Fe core during the synthesis (Ai et al., 2007a). The core–shell Fe@Fe_2O_3 nanonecklace was very stable in air because of the protection of oxide shell. This stability is very important for constructing an electrochemical biosensor.

The fabrication processes of the film were monitored by cyclic voltammetry (CV) of 1.0 mmol L^{-1} $[Fe(CN)_6]^{3-/4-}$ (1:1) in 0.1 mol L^{-1} KCl (see supplementary material Fig. S1). Well-defined cyclic voltammogram and characteristics of a diffusion-controlled redox process were observed at the bare GCE (curve a) with

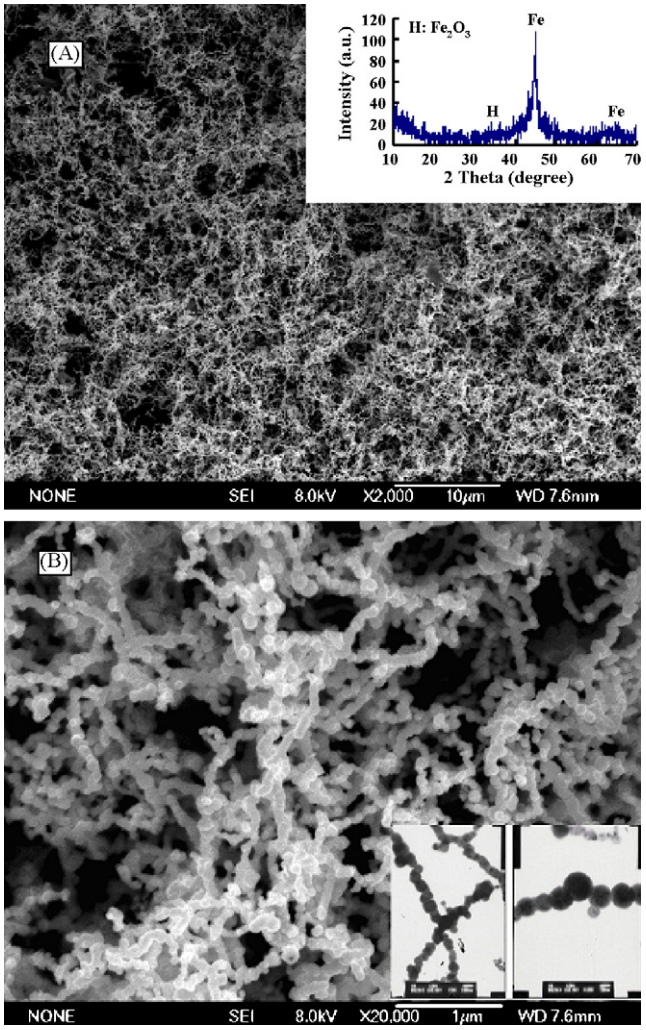

Fig. 1. The SEM images at low magnification (A) and high magnification (B) of as-prepared Fe@Fe_2O_3 core–shell nanonecklace. The inset of A and inset of B are the XRD pattern and the TEM images of as-prepared Fe@Fe_2O_3 core–shell nanonecklace, respectively.

the cathodic peak current $i_{pc} = (1.797 \pm 0.06) \times 10^{-5}$ A and the anodic peak current $i_{pa} = (-1.834 \pm 0.04) \times 10^{-5}$ A. The cathodic potential E_{pc} and the anodic potential E_{pa} were 144 ± 2 mV and 229 ± 2 mV, respectively. The peak-to-peak separation ΔE_p was 85 ± 4 mV. After PDDA was immobilized on the surface of the GCE, both the cathodic peak $[(3.713 \pm 0.07) \times 10^{-5}$ A] and anodic peak $[(-1.860 \pm 0.06) \times 10^{-5}$ A] of $[Fe(CN)_6]^{3-/4-}$ increased (curve b) due to the affinity of the positively charged PDDA to $[Fe(CN)_6]^{3-/4-}$. With the assembly of the mixture of Fe@Fe_2O_3 core–shell nanonecklace and Au nanoparticles, the peak currents increased further $i_{pc} = (4.011 \pm 0.1) \times 10^{-5}$ A and $i_{pa} = (-2.104 \pm 0.06) \times 10^{-5}$ A and the ΔE_p became to be 79 ± 5 mV (curve c), which could be ascribed to the good conductivity and the large surface area of the nanoparticles. After another layer of PDDA was modified, the peak currents became much larger $[i_{pc} = (7.168 \pm 0.12) \times 10^{-5}$ A and $i_{pa} = (-4.301 \pm 0.08) \times 10^{-5}$ A] and the ΔE_p (74 ± 4 mV) much smaller (curve d). When ds-DNA was modified on the electrode, the peak currents decreased apparently and the ΔE_p became larger because of the repulsion between DNA and $[Fe(CN)_6]^{3-/4-}$. The i_{pc} and the i_{pa} were $(3.632 \pm 0.04) \times 10^{-5}$ A and $(-2.282 \pm 0.04) \times 10^{-5}$ A, respectively, and the ΔE_p was 128 ± 6 mV (curve e). All above the values of the peak currents and the potentials were average values of three parallel measurements.

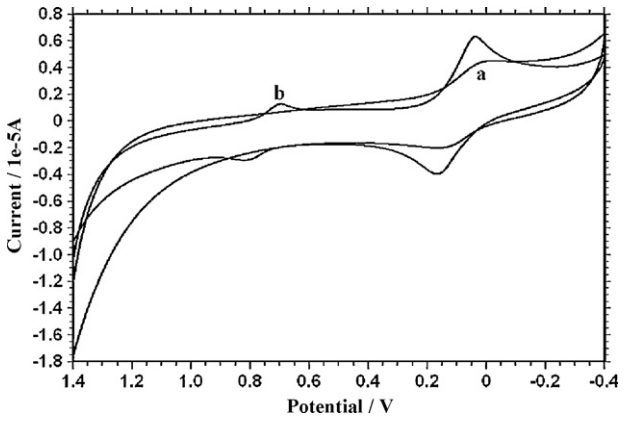

Fig. 2. Cyclic voltammograms of 50 mmol L^{-1} $Ru(NH_3)_6^{3+}$ in 0.1 mol L^{-1} PBS of pH 5.5 at DNA/PDDA/Fe@Fe_2O_3–Au/PDDA/GCE before (a) and after (b) the cathodic treatment for 30 min. Scan rate: 100 mV s^{-1}.

3.2. Electrochemical measurements of the DNA damage

3.2.1. $Ru(NH_3)_6^{3+}$ as the probe

Fig. 2 shows the cyclic voltammograms of 50 mmol L^{-1} $Ru(NH_3)_6^{3+}$ in 0.1 mol L^{-1} PBS of pH 5.5 at DNA/PDDA/Fe@Fe_2O_3–Au/PDDA/GCE before (curve a) and after (curve b) the cathodic treatment. There are a couple of well-defined redox peaks at −0.020 V and 0.169 V, respectively, in curve a, which were the redox peaks of the iron ions leaching from Fe@Fe_2O_3 core–shell nanonecklace (Ai et al., 2007a). After a cathodic process, a new couple of well-defined redox peaks appeared at 0.697 V and 0.758 V, respectively (curve b). At the same time the redox peaks of the iron ions became larger compared with curve a, which could be ascribed to more iron ions leaching from Fe@Fe_2O_3 nanonecklace after the treatment. The new redox peaks corresponded to the catalytic redox cycle of $Ru(NH_3)_6^{3+}$. When ds-DNA in the film was damaged *in situ* by the hydroxyl radical electrogenerated during the cathodic treatment, the guanines released from the protection of the double helix were easily oxidized by $Ru(NH_3)_6^{3+}$ and the formed $Ru(NH_3)_6^{2+}$ was then electrooxidized, resulting in a catalytic cycle. The catalytic current of $Ru(NH_3)_6^{3+}$ can be readily utilized for the detection of DNA damage.

During the course of the cathodic treatment, the Au nanoparticles were used as electrocatalysts for H_2O_2 electrogeneration (Eq. (1)). According to Villers et al. (2006), the ideal electrocatalysts for H_2O_2 electrogeneration should meet three demands: a high electrical conductivity, easy accessibility for the reactant gas to the electrocatalyst, and good corrosion resistance, especially under the highly oxidizing conditions. The Au nanoparticles have many good properties such as good electrical conductivity, relative chemical inertness to most electrolyte solutions, high surface activity, and a wide operational potential window, so it was ideal electrocatalysts for H_2O_2 electrogeneration. In additional, the Fe@Fe_2O_3 core–shell nanonecklace, which was mixed with Au nanoparticles in this system, has strong adsorption for oxygen dissolved in the solution due to their porous structure. These two aspects made the process of the Eq. (1) very easy.

The Fe@Fe_2O_3 core–shell nanonecklace reacted with H^+ according to reactions (Eqs. (2) and (3)). These reactions would release Fe^{3+} and/or Fe^{2+} from the Fe@Fe_2O_3 core–shell nanonecklace. Moreover, under aerobic conditions, the reaction (4) might take place. The Fe^{2+} reacted with H_2O_2 to generate hydroxyl radical, the so-called Fenton reaction (Eq. (6)). The generated Fe^{3+} could be returned to Fe^{2+} by the direct reduction of Fe^{3+} at the electrode (Eq. (5)), or by the reaction with H_2O_2 (Eq. (7)), (Ai et al., 2007a,b). So the Fe^{2+} was recycling. The hydroxyl radical generated in the Fenton reaction attacked DNA in the film and induced DNA damage *in situ*. When the $Ru(NH_3)_6^{3+}$ was used as electroactive indicator, the exposed guanine from the protection of ds-DNA double helix would be oxidized, resulting in a redox catalytic cycle (Eqs. (8)–(10)) (Zhou and Rusling, 2001; Mugweru and Rusling, 2002; Konnann et al., 1988). So a couple of new redox peaks appeared (curve b).

$$O_2 + 2H^+ + 2e^- \underset{\text{Cathodic process}}{\xrightarrow{\text{Au}}} H_2O_2 \quad (1)$$

$$Fe_2O_3 + 6H^+ \rightarrow 2Fe^{3+} + 3H_2O \quad (2)$$

$$Fe^0 + 2H^+ \rightarrow Fe^{2+} + H_2 \quad (3)$$

$$2Fe^0 + O_2 + 2H_2O \rightarrow 2Fe^{2+} + 4OH^- \quad (4)$$

$$Fe^{3+} + e^- \rightarrow Fe^{2+} \quad (5)$$

$$Fe^{2+} + H_2O_2 \rightarrow Fe^{3+} + {}^{\bullet}OH + OH^- \quad (6)$$

$$Fe^{3+} + H_2O_2 \rightarrow Fe^{2+} + {}^{\bullet}HO_2 + H^+ \quad (7)$$

$$\text{ds-DNA} \xrightarrow{{}^{\bullet}OH\ \text{attack}} \text{DNA(guanine)} \quad (8)$$

$$Ru(NH_3)_6^{3+} + \text{DNA(guanine)} \rightarrow Ru(NH_3)_6^{2+} + \text{DNA(guanine}^+) \quad (9)$$

$$Ru(NH_3)_6^{2+} = Ru(NH_3)_6^{3+} + e^- \quad (10)$$

DPV was used for the detection of DNA damage *in situ* due to its higher sensitivity than the CV. The DPV changes of $Ru(NH_3)_6^{3+}$ at the biosensor with the time of the cathodic treatment are shown in Fig. 3. When the film was not treated by a cathodic process (0 min), a very little peak of $Ru(NH_3)_6^{3+}$ at 0.740 V was found. The peak current increased with the time of the cathodic treatment and reached the biggest at 48 min. The peak increased at a relatively larger rate within the first 10 min of the cathodic treatment, which demonstrated that the DNA damage was the most severe within the first 10 min. For the controlled experiments that the modified electrode was set in the same solution but without the cathodic treatment for the same time, the peak currents of $Ru(NH_3)_6^{3+}$ had no change.

The ratio of Fe@Fe_2O_3 core–shell nanonecklace to Au nanoparticles had a pronounced effect on the DNA damage. Different volume ratios of Fe@Fe_2O_3 core–shell nanonecklace to Au nanoparticles (with 1.5 mg mL^{-1} and 3.0×10^{-9} mol L^{-1} concentrations, respectively), such as 0:40, 5:35, 10:30, 15:25, 20:20, 25:15, 30:10, 35:5 and 40:0, were tested. The performance of the biosensor was characterized by DPV in 0.1 mol L^{-1} PBS of pH 5.5 containing 50 mmol L^{-1} $Ru(NH_3)_6^{3+}$. The DPV current change ΔI_p of $Ru(NH_3)_6^{3+}$ before and after the cathodic treatment for 30 min was obtained. The dependence of the volume ratio of Fe@Fe_2O_3

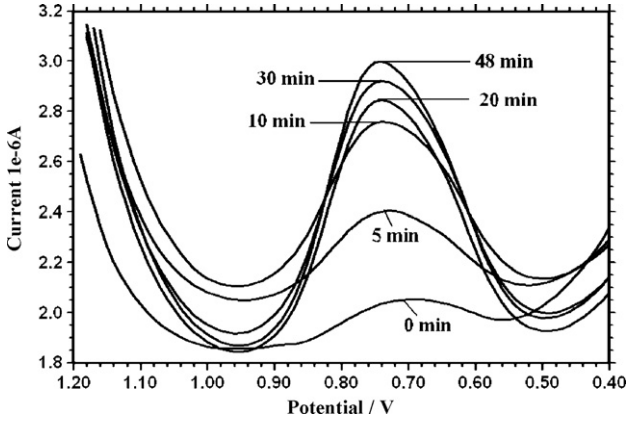

Fig. 3. Differential pulse voltammograms of 50 mmol L^{-1} $Ru(NH_3)_6^{3+}$ in 0.1 mol L^{-1} PBS of pH 5.5 at DNA/PDDA/Fe@Fe_2O_3–Au/PDDA/GCE by the cathodic treatment for different times.

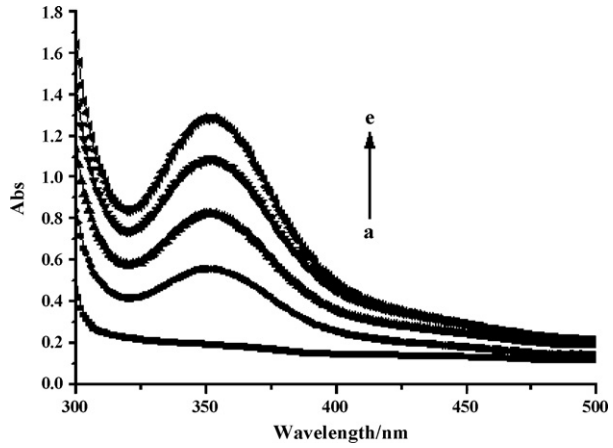

Fig. 4. Dependence of UV–vis spectrum of H_2O_2 on the cathodic treatment time: 0 min (a); 10 min (b); 20 min (c); 30 min (d); 40 min (e).

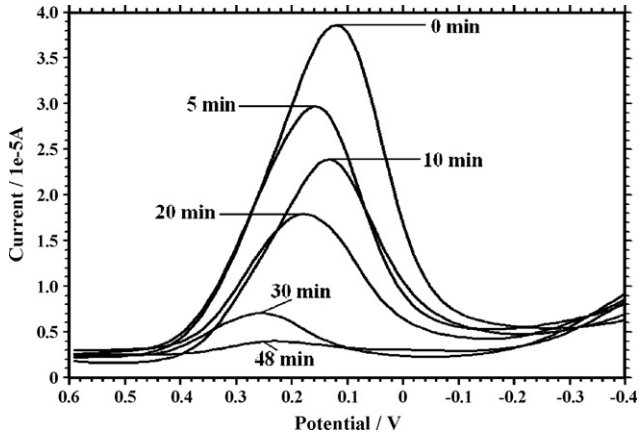

Fig. 5. Differential pulse voltammograms of 20 mmol L^{-1} $Co(phen)_3^{3+}$ in 0.1 mol L^{-1} PBS of pH 5.5 at DNA/PDDA/$Fe@Fe_2O_3$–Au/PDDA/GCE by the cathodic process for different times.

core–shell nanonecklace to Au nanoparticles on ΔI_p is shown in supplementary material (Fig. S2). The histogram shows that the ΔI_p increased with the increasing ratio of $V_{Fe@Fe_2O_3}$: $V_{Au\ NPs}$ and reached a maximum value at the ratio of 10:30. After that, the ΔI_p decreased. When the ratio of $Fe@Fe_2O_3$ core–shell nanonecklace to Au nanoparticles was 0:40 or 40:0, the ΔI_p was very small, which demonstrated that $Fe@Fe_2O_3$ core–shell nanonecklace and Au nanoparticles played considerable synergistic effects for DNA damage. The optimal ratio of $V_{Fe@Fe_2O_3}$: $V_{Au\ NPs}$ was 10:30.

The influence of the pH value in cathodic treatment process on DNA damage was investigated in the range of pH 4.0–7.0 also via recording the DPV curves of $Ru(NH_3)_6^{3+}$ before and after treatment. The experimental results indicated that the largest ΔI_p could be obtained under weak acidic conditions (pH 5.0–5.8) than at other pHs at room temperature. If the pH value was too low, the $Fe@Fe_2O_3$ core–shell nanonecklace would be dissolved and the film would peel off from the surface of the electrode. Therefore, pH 5.5 was selected as the optimal pH for the cathodic process.

The analysis of H_2O_2 produced in the cathodic process was carried out using the UV–vis spectrum with off-line sampling (Konnann et al., 1988). The absorption at 352 nm was linearly dependent on H_2O_2 concentration in the solution. The results are shown in Fig. 4. It could be seen that there was no absorption at 352 nm at beginning of the cathodic treatment, showing no H_2O_2 generation, and that the concentration of H_2O_2 successively grew with the increase of the treatment time at almost a constant rate. The concentration of the iron ions produced during the course of the cathodic treatment was determined by classical spectrophotometry using 1,10-phenanthroline. The procedure was as follows: 1 mL of 10% hydroxylamine hydrochloride (prepared freshly), 2 mL of 1.0×10^{-3} mol L^{-1} 1,10-phenanthroline and 1 mL sample solution treated by cathodic process were mixed thoroughly. After standing for 10 min, the absorption at 510 nm was determined. The results showed that iron ions could also be produced at almost a constant rate from the film during the course of the cathodic treatment. The electrogeneration of H_2O_2 and the iron ions at a constant rate was greatly favorable for a controlled damage of DNA.

To account for electrode-to-electrode reproducibility, seven different modified electrodes were independently fabricated in the same way and were used to detect the DNA damage. The ΔI_p on every electrode before and after the E-Fenton reaction for 30 min was obtained and the relative standard deviation (RSD) of seven ΔI_ps was 2.37%. The results revealed that the biosensor had good reproducibility. The long-term stability was an important parameter for evaluation of the performance of the biosensor. By comparing the difference of ΔI_ps between a new fabricated biosensor and a stored biosensor in the air for 15 days at room temperature, the long-term stability of the biosensor was evaluated. The results showed that the mean deviation was less than 5% ($n = 5$), showing the good stability of the biosensor. The regeneration of this biosensor was also studied. After the detection, the biosensor was treated at −0.6 V for 1 min, then it was washed with pH 7.0 PBS containing 0.5% sodium dodecylsulfate (SDS) solution and ultrapure water in sequence, so that the DNA was removed from the surface of the modified electrode. Subsequently, the electrode was coated again with 2.0 mg mL^{-1} of ds-DNA 8.0 μL. This regenerated sensor can be used for detecting the DNA damage. After this course was repeated for 7 times, the detection signal was about 95% of the first measurement signal. Therefore, this biosensor had good operational stability.

The minimal detectable amount of DNA damage was determined by coating the modified electrode with different concentrations of 8.0 μL ds-DNA and measuring the DPV current change ΔI_p of $Ru(NH_3)_6^{3+}$ before and after the cathodic treatment for 30 min. The experiments showed that the minimal detectable concentration of ds-DNA damage was 0.05 mg mL^{-1}. So the threshold of DNA damage was 0.4 μg.

3.2.2. $Co(phen)_3^{3+}$ as the probe

$Co(phen)_3^{3+}$ can also be used as an electroactive probe to detect DNA damage. $Co(phen)_3^{3+}$ binds more strongly with the intact ds-DNA in the film than the damaged DNA owing to the intercalative binding of $Co(phen)_3^{3+}$ to ds-DNA. This method might be an alternative in situations where oxidizable interferences were encountered. After the biosensor was treated by a cathodic process for a given time, the electrode was washed and placed into a 20 mmol L^{-1} $Co(phen)_3^{3+}$ solution and DPV signals were recorded. Fig. 5 shows that the largest peak for the reduction of $Co(phen)_3^{3+}$ at 0.12 V was obtained for the intact ds-DNA (0 min), because of the largest amount binding of $Co(phen)_3^{3+}$ with the intact ds-DNA. The peak currents decreased with the time of the cathodic treatment, which suggested that the ability of the film to bind the probe was gradually losing and the DNA damage was becoming more severe. The controlled experiments illustrated that the peak currents of $Co(phen)_3^{3+}$ have no change if there was no the cathodic treatment.

4. Conclusion

$Fe@Fe_2O_3$ core–shell nanonecklace and Au nanoparticle were prepared and an electro-Fenton reaction based on these two nanoparticles was used for electrochemical sensing of rapid detection and mimicking metal-mediated DNA damage *in situ*. The two

Fenton reagents, iron ion and H_2O_2, were produced *in situ* from $Fe@Fe_2O_3$ core–shell nanonecklace and oxygen reduction on the Au nanoparticle surface, respectively, when the electrode was treated by a cathodic process. The DNA damage was monitored by cyclic voltammetry and differential pulse voltammetry with $Ru(NH_3)_6^{3+}$ (or $Co(phen)_3^{3+}$ as an alternative) as electroactive probe. The performance of the biosensor was very excellent. All in all, the work presented here has demonstrated that the electrochemical strategy for mimicking the metal-mediated DNA damage *in situ* by E-Fenton reaction based on $Fe@Fe_2O_3$ core–shell nanonecklace and Au nanoparticles is feasible. This approach allowed detection of damaged DNA in the films within 5–10 min of incubation with the cathodic treatment.

Acknowledgements

We are grateful to the financial support of the National Natural Science Foundation of China (20635020 and 20805025) and Doctorial Foundation of the Ministry of Education of China (No. 20060426001) and Doctoral Fund of QUST (0022278).

Appendix A. Supplementary data

Supplementary data associated with this article can be found, in the online version, at doi:10.1016/j.bios.2009.04.026.

References

Ai, Z.H., Liu, L.R., Li, J.P., Jia, F.L., Zhang, L.Z., Qiu, J.R., 2007a. J. Phys. Chem. C 111, 14799–14803.
Ai, Z.H., Mei, T., Liu, J., Li, J.P., Zhang, L.Z., Qiu, J.R., Wu, M.H., 2007b. J. Phys. Chem. C 111, 4087–4093.
Cooke, M.S., Evans, M.D., Dizdaroglu, M., Lunec, J., 2003. FASEB J. 17, 1195–1214.
Dollimore, L.S., Gillard, R.D., 1973. J. Chem. Soc., Dalton Trans. 9, 933–940.
Feng, Y.Y., Yang, T., Zhang, W., Jiang, C., Jiao, K., 2008. Anal. Chim. Acta 616, 144–146.
Jia, S.P., Liang, M.M., Guo, L.H., 2008. J. Phys. Chem. B 112, 4461–4464.
Konnann, C., Bahnemann, D., Hofmann, M.R., 1988. Environ. Sci. Technol. 22, 798–806.
Liang, M.M., Guo, L.H., 2007. Environ. Sci. Technol. 41, 658–664.
Liang, M.M., Jia, S.P., Zhu, Sh.Ch., Guo, L.H., 2008. Environ. Sci. Technol. 42, 635–639.
Mugweru, A., Jing, Y., Rusling, J.F., 2004. Electroanalysis 16, 1132–1138.
Mugweru, A., Rusling, J.F., 2002. Anal. Chem. 74, 4044–4094.
Palecék, E., Fojta, M., Tomschik, M., Wang, J., 1998. Biosens. Bioelectron. 13, 621–628.
Shosuke, K., Yusuke, H., Mariko, M., Shinji, O., 2002. Free Radical Biol. Med. 32, 822–832.
So, M., Hvastkovs, E.G., Bajrami, B., Schenkman, J.B., Rusling, J.F., 2008. Anal. Chem. 80, 1192–1200.
Storhoff, J.J., Elghanian, R., Mucic, R.C., Mirkin, C.N., Letsinger, R.L., 1998. J. Am. Chem. Soc. 120, 1959–1964.
Tarun, M., Bajrami, B., Rusling, J.F., 2006. Anal. Chem. 78, 624–627.
Tarun, M., Rusling, J.F., 2005. Crit. Rev. Eukaryot. Gene Expr. 15, 295–315.
Villers, D., Sun, S.H., Serventi, A.M., Dodelet, J.P., 2006. J. Phys. Chem. B 110, 25916–25925.
Xue, W.L., Warshawsky, D., 2005. Toxicol. Appl. Pharmacol. 206, 73–93.
Zhou, L.P., Estavillo, C., Stuart, J.D., Schenkman, J.B., Rusling, J.F., 2003. J. Am. Chem. Soc. 125, 1431–1436.
Zhou, L.P., Rusling, J.F., 2001. Anal. Chem. 73, 4780–4786.